

Electronic Supplementary Information

Photovoltaic mixed-cation lead mixed-halide perovskites: Links between crystallinity, photo-stability and electronic properties

Waqas Rehman, David P. McMeekin, Jay B. Patel, Rebecca L. Milot, Michael B. Johnston, Henry J. Snaith and Laura M. Herz*

Table of Contents

A. Materials, Synthesis and Film Fabrication	p.2
B. Experimental techniques and analysis	p.3
B1. Optical pump - THz probe spectroscopy	p.3
B2. Global Fits to THz photoconductivity transients	p.3
B3. Derivation of photoconductivity and charge carrier mobility from change in THz electric field transmission	p.4
B4. Time-resolved photoluminescence (PL)	p.5
B5. X-ray Diffraction (XRD)	p.6
C. Further characterization data for $\text{Cs}_y\text{FA}_{(1-y)}\text{Pb}(\text{Br}_{0.4}\text{I}_{0.6})_3$	p.7
C1. XRD data for $\text{Cs}_y\text{FA}_{(1-y)}\text{Pb}(\text{Br}_{0.4}\text{I}_{0.6})_3$ and $\text{Cs}_y\text{FA}_{(1-y)}\text{PbI}_3$ films	p.7
C2. PL and absorption spectra for $\text{Cs}_y\text{FA}_{(1-y)}\text{Pb}(\text{Br}_{0.4}\text{I}_{0.6})_3$ films	p.10
C3. PL transients for $\text{Cs}_y\text{FA}_{(1-y)}\text{Pb}(\text{Br}_{0.4}\text{I}_{0.6})_3$ films	p.12
C4. PL photodegradation spectra for selected $\text{Cs}_y\text{FA}_{(1-y)}\text{Pb}(\text{Br}_{0.4}\text{I}_{0.6})_3$ films	p.13
D. Further characterization data for $\text{Cs}_{0.17}\text{FA}_{0.83}\text{Pb}(\text{Br}_x\text{I}_{(1-x)})_3$ films	p.14
D1. PL transients for $\text{Cs}_{0.17}\text{FA}_{0.83}\text{Pb}(\text{Br}_x\text{I}_{(1-x)})_3$ films	p.14
D2. THz photoconductivity transients for $\text{Cs}_{0.17}\text{FA}_{0.83}\text{Pb}(\text{Br}_x\text{I}_{(1-x)})_3$ films	p.15
D3. PL and absorption spectra for $\text{Cs}_{0.17}\text{FA}_{0.83}\text{Pb}(\text{Br}_x\text{I}_{(1-x)})_3$ films	p.16
D4. Calculation of charge-carrier diffusion lengths $\text{Cs}_{0.17}\text{FA}_{0.83}\text{Pb}(\text{Br}_x\text{I}_{(1-x)})_3$ films	p.18

A. Materials, Synthesis and Film Fabrication

Materials: Unless otherwise stated, all materials were purchased from Sigma-Aldrich or Alfa Aesar and used as received.

Perovskite precursor synthesis: Formamidinium iodide (FAI) was synthesised by dissolving formamidine acetate powder in a 1.5x molar excess of 57%w/w hydroiodic acid (HI). After addition of acid the solution was left stirring for 10 minutes at 50°C and dried at 100°C for 2h, or until a yellow-white powder was formed. This was then washed three times with diethyl ether. The powder was later dissolved in ethanol and heated at 100°C to obtain a supersaturate solution. Once fully dissolved, the solution was then placed in a refrigerator for overnight recrystallization. The recrystallization process resulted in white flake-like crystals. The powder was later washed with diethyl ether three times. Finally, the powder was dried overnight in a vacuum oven at 50°C.

Perovskite precursor solution mixture: Solutions were prepared using FAI, FAb, CsI and CsBr, PbBr₂ and PbI₂ which were dissolved in anhydrous N,N-dimethylformamide (DMF) to yield a stoichiometric solution with desired Cs_(y)FA_(1-y)Pb(Br_(x)I_(1-x))₃ composition. All solutions were aged for approximately 48h after addition of HI, HBr or a mixture of both. Acid concentrations were adjusted according to the molarity of the solution and the halide composition of the precursor salts. To obtain a series of Cs_(y)FA_(1-y)Pb(Br_{0.4}I_{0.6})₃ precursor solutions, we mixed two stoichiometric precursor solutions with fixed 40/60 Br/I halide ratios, but with various FA/Cs cation ratios. For compositions ranging from 0 to 30% Cs, we mixed a 0.95M solution of FAPb(Br_{0.4}I_{0.6})₃ with a 0.95M Cs_{0.3}FA_{0.7}Pb(Br_{0.4}I_{0.6})₃. For compositions ranging from 40 to 100% Cs, we mixed a 0.2M CsPb(Br_{0.4}I_{0.6})₃ with the 0.95M Cs_{0.3}FA_{0.7}Pb(Br_{0.4}I_{0.6})₃ solution, because of the lower solubility of cesium salts in DMF. Volume ratios between the two solutions were adjusted to obtain the desired compositions. 55μl of 57%w/w hydroiodic acid (HI) and 27μl of 48%w/w hydrobromic acid (HBr) were added to 1ml of 0.95M precursor solutions, while 11.6μl of HI and 4.8μl of HBr were added to 1ml of 0.2M precursor solution under a N₂ atmosphere. To obtain a series of Cs_{0.17}FA_{0.83}Pb(Br_(x)I_(1-x))₃ precursor solutions, we mixed two stoichiometric precursor solutions with fixed 83/17 FA/Cs cation ratios, but with various Br/I halide ratios. For compositions ranging from 0 to 50% Br, a 0.95M solution Cs_{0.17}FA_{0.83}PbI₃ with 91μl of HI per ml of solution was mixed with a 0.95M Cs_{0.17}FA_{0.83}Pb(Br_{0.6}I_{0.4})₃ with 34.2μl of HBr and 45.6μl HI per ml of solution. For compositions ranging from 60% to 100% Br, a 0.2M

solution $\text{Cs}_{0.17}\text{FA}_{0.83}\text{PbBr}_3$ with 14.4 μl of HBr per ml of solution was mixed with the 1ml of 0.95M $\text{Cs}_{0.17}\text{FA}_{0.83}\text{Pb}(\text{Br}_{0.6}\text{I}_{0.4})_3$ solution.

Thin-film fabrication: The precursor perovskite solution was spin-coated in a nitrogen-filled glovebox at 2000rpm for 45s, on a substrate pre-heated at 70°C. Immediately after spin-coating, the films were dried inside a N_2 glovebox on a hot plate at a temperature of 70°C for 1 minute. All films, with the exception of $\text{CsPb}(\text{Br}_{0.4}\text{I}_{0.6})_3$, were then annealed in an oven in an air atmosphere at 185°C for 90 minutes. $\text{CsPb}(\text{Br}_{0.4}\text{I}_{0.6})_3$ films were annealed inside N_2 at 185°C for 30m.

B. Experimental techniques and analysis

B1. Optical pump - THz probe spectroscopy

The optical-pump-THz-probe setup uses a Spectra Physics Ti:Sapphire regenerative amplifier to generate 40 fs pulses at a center wavelength of 800 nm and a repetition rate of 1.1kHz. Terahertz pulses were generated by optical rectification in a 450 μm thick GaP(110) single crystal and detected by electro-optic sampling in a ZnTe crystal (0.2mm (110)-ZnTe on 3mm (100)-ZnTe). Pulses for optical excitation of the samples at 400nm have been generated using a beta barium borate frequency doubling crystal. Optical excitation was carried out from the substrate side of the film. The diameters of optical pump and THz probe beams at the sample position were 3.6 mm and 2.4 mm (FWHM), respectively. Measurements were performed with the entire THz beam path (including emitter, detector and sample) in an evacuated chamber at a pressure of $<10^{-2}$ bar.

B2. Global Fits to THz photoconductivity transients

The recombination dynamics of the free charge-carrier density $n(t)$ is determined by first, second and third order decay mechanisms and described by the following rate equation, also provided in the main manuscript,

$$\frac{dn(t)}{dt} = -k_3 n^3 - k_2 n^2 - k_1 n \quad (6)$$

The experimentally observed quantity of photoinduced THz transmission change $x(t) = \left(\frac{\Delta T}{T}\right)(t)$ is linearly related to the free charge-carrier in the form of

$$n(t) = \varphi C x(t) \quad (7)$$

Hence, $C = n_0/x(0)$ is the proportionality factor between the immediate THz response $x(0)$ and the initially absorbed photon density n_0 with

$$n_0 = \frac{E \lambda \alpha(\lambda)}{hc A_{eff}} (1 - R_{pump}) \quad (8)$$

which can be derived from pump beam parameters and the absorption coefficient α at our excitation wavelength of 400 nm. If (6) is substituted into (5) we obtain the following relation

$$\begin{aligned} \frac{dn(t)}{dt} &= -C^2 \varphi^2 k_3 x^3 - C \varphi k_2 x^2 - k_1 x \\ &= -A_3 x^3 - A_2 x^2 - A_1 x \end{aligned} \quad (9)$$

with $A_i = C^{i-1} \varphi^{i-1} k_i$. Taking a fluence dependent set of THz photoconductivity transients belonging to a particular film, numerical solutions according equation (8) are fitted simultaneously to all transients. Therefore, there is only one globally optimized value for A_i applied to all fluences. As we can expect a spatially varying charge density profile, our fit routine also considers the exponential charge density profile created by the pump beam. The sample is divided into 30 equally thick slices and the decay function is computed for all of these individually.

B3. Derivation of photoconductivity and charge carrier mobility from change in THz electric field transmission

Assuming the thickness of the perovskite film is smaller than the THz wavelength, the sheet photoconductivity ΔS of a thin film between two media of refractive indices n_a and n_b can be expressed as

$$\Delta S = -\epsilon_0 c (n_a + n_b) \frac{\Delta T}{T} \quad (1)$$

where the product $\epsilon_0 c$ denotes the invert of the vacuum impedance and $\Delta T/T$ the photoinduced change in THz electric field transmission over total transmission. As the experiment has been performed in an evacuated box under vacuum, the samples are surrounded by vacuum from one side ($n_b = 1$) and in direct contact with the z-cut quartz substrate from the other side ($n_a = 2.13$) through which the photoexcitation of the sample occurs.

The charge-carrier mobility μ can be calculated as follows

$$\mu = \frac{\Delta S A_{eff}}{N e} \quad (2)$$

where ΔS is the sheet photoconductivity of a thin film, e is the elementary charge and N is the number of photoexcited charge-carriers. A_{eff} is the effective area of the overlap of optical pump and THz probe pulse calculated as follows

$$A_{eff} = \frac{\pi}{\ln(2)} (FWHM_{pump}^2 + FWHM_{probe}^2) \quad (3)$$

The number of photoexcited charge-carriers N can be determined as follows

$$N = \varphi \frac{E\lambda}{hc} (1 - R_{pump}) (1 - T_{pump}) \quad (4)$$

where φ is the ratio of charge-carriers produced following photon absorption, also known as the photon-to-charge branching ratio, which is assumed to be unity. E , is the energy contained in an optical excitation pulse of wavelength λ , R_{pump} is the reflectivity of the sample at normal incidence of the excitation beam, T_{pump} denotes for the portion of pump beam which is transmitted through the sample. As φ is declared unknown, we define an effective mobility $\tilde{\mu} = \varphi\mu$ which can be directly obtained from our experiments

$$\varphi\mu = -\varepsilon_0 c (n_a + n_b) \frac{A_{eff} hc}{E e \lambda (1-R_{pump}) (1-T_{pump})} \frac{\Delta T}{T} \quad (5)$$

The ascertained charge-carrier mobility contains contributions from both electrons and holes. Hence, the derived values for mobility represent the sum of electron and hole mobilities. As φ ranges between 0 and 1, the effective mobility describes a lower limit.

B4. Time-resolved photoluminescence (PL)

Time-resolved PL spectroscopy by means of time-correlated single photon counting (TCSPC) was performed to determine monomolecular recombination rate constants k_1 . A picosecond pulsed diode laser (Picoquant, LDH-D-C-405M) centered at 400 nm was used to photoexcite the sample. The PL was collected and directed toward a grating monochromator (Princeton Instruments, SP-2558) fitted with a photon counting detector (PDM series from MPD). The timing was controlled with a PicoHarp300 time-correlated single photon counting (TCSPC)

event timer. Measurements were undertaken at very low excitation fluence where higher order processes are assumed to be negligible. Monomolecular recombination rates k_1 were extracted through mono-exponential fits to the tails of the low-fluence PL decay traces of each film as shown in **Figures S6 and S8**. While curves were acquired at lowest possible fluences and acquired reasonably quickly, some light-induced segregation may influence the PL traces creating additional error in the extracted monomolecular recombination rates k_1 . However, the bimolecular and Auger rates are determined through THz transient photoconductivity spectroscopy at much higher excitation intensity and are not affected, as discussed in the main text.

B5. X-Ray diffraction (XRD)

X-ray diffraction was using an X-ray diffractometer (Panalytical X'Pert Pro). The scan speed was 0.01 °/s for 90 minutes (Cu-K α radiation operating at 40 kV and 40 mA). Peak fitting was carried using Highscore Plus software. Essentially the peaks were fitted with a Pearson VII fit then shifted to correspond to the quartz reference peak ($2\theta=16.43^\circ$). Parameters were then extracted from these fits.

C. Further characterization data for $\text{Cs}_y\text{FA}_{(1-y)}\text{Pb}(\text{Br}_{0.4}\text{I}_{0.6})_3$

C1. XRD data for $\text{Cs}_y\text{FA}_{(1-y)}\text{Pb}(\text{Br}_{0.4}\text{I}_{0.6})_3$ and $\text{Cs}_y\text{FA}_{(1-y)}\text{PbI}_3$ films

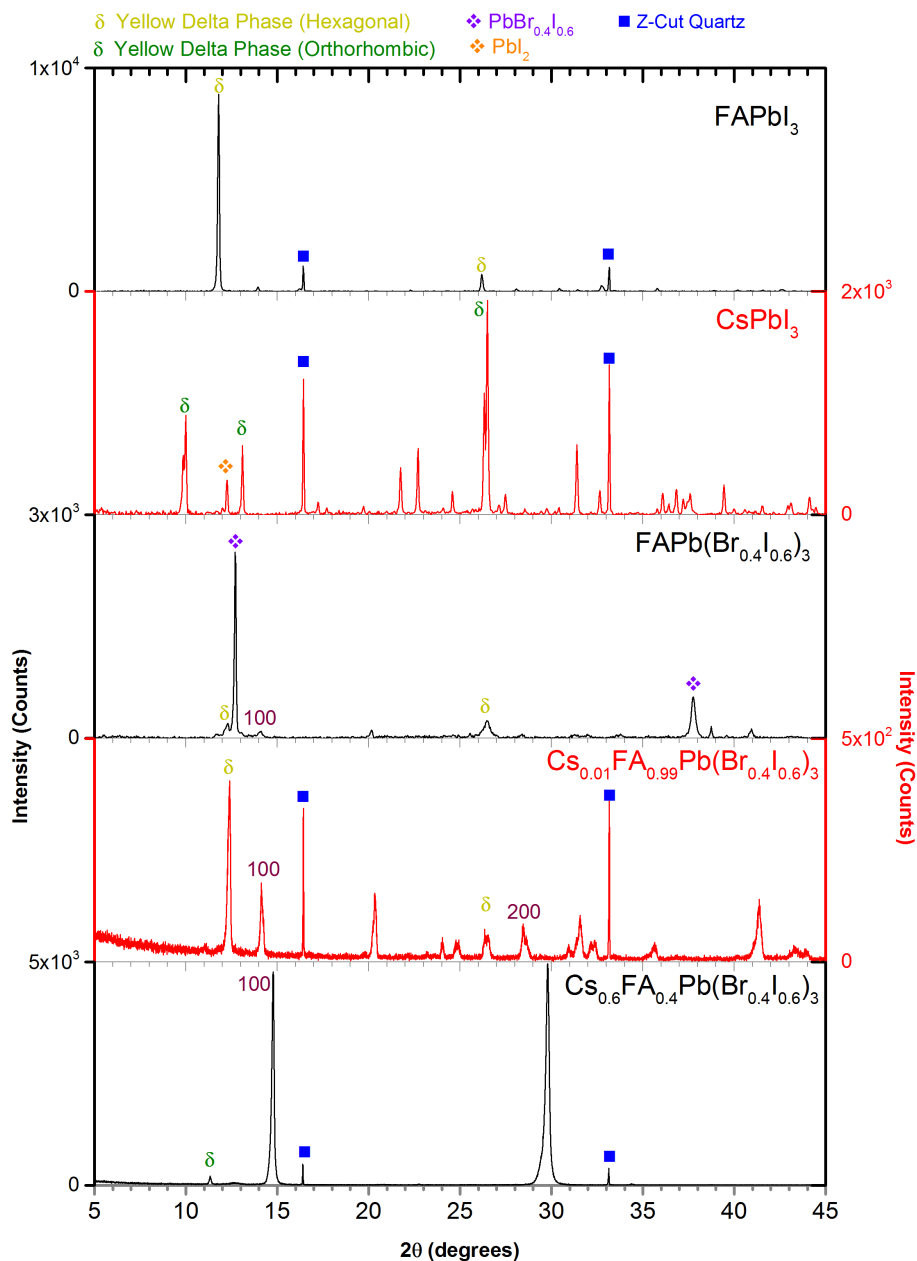


Figure S1. X-ray Diffraction patterns of δ -phase FAPbI₃, δ -phase CsPbI₃, yellow FAPb(Br_{0.4}I_{0.6})₃ and the 1% and 60% Cs films used in the study. From the diffraction pattern obtained for the FAPb(Br_{0.4}I_{0.6})₃, there are clear reflections from some excess PbI₂ ($2\theta=12.7^\circ$) and the hexagonal yellow phase of the mixed halide FAPb(Br_{0.4}I_{0.6})₃ ($2\theta=12.4^\circ$). The substitution of iodine with bromine results in a contraction of the lattice volume, which explains the shift to a larger 2θ angle from the original hexagonal yellow FAPbI₃ reflection ($2\theta=11.8^\circ$). This enables us to assign the reflection observed at $2\theta=12.4^\circ$ with the yellow hexagonal FAPb(Br_{0.4}I_{0.6})₃, which are observed in films with very small quantities of Cs (0%-5%).

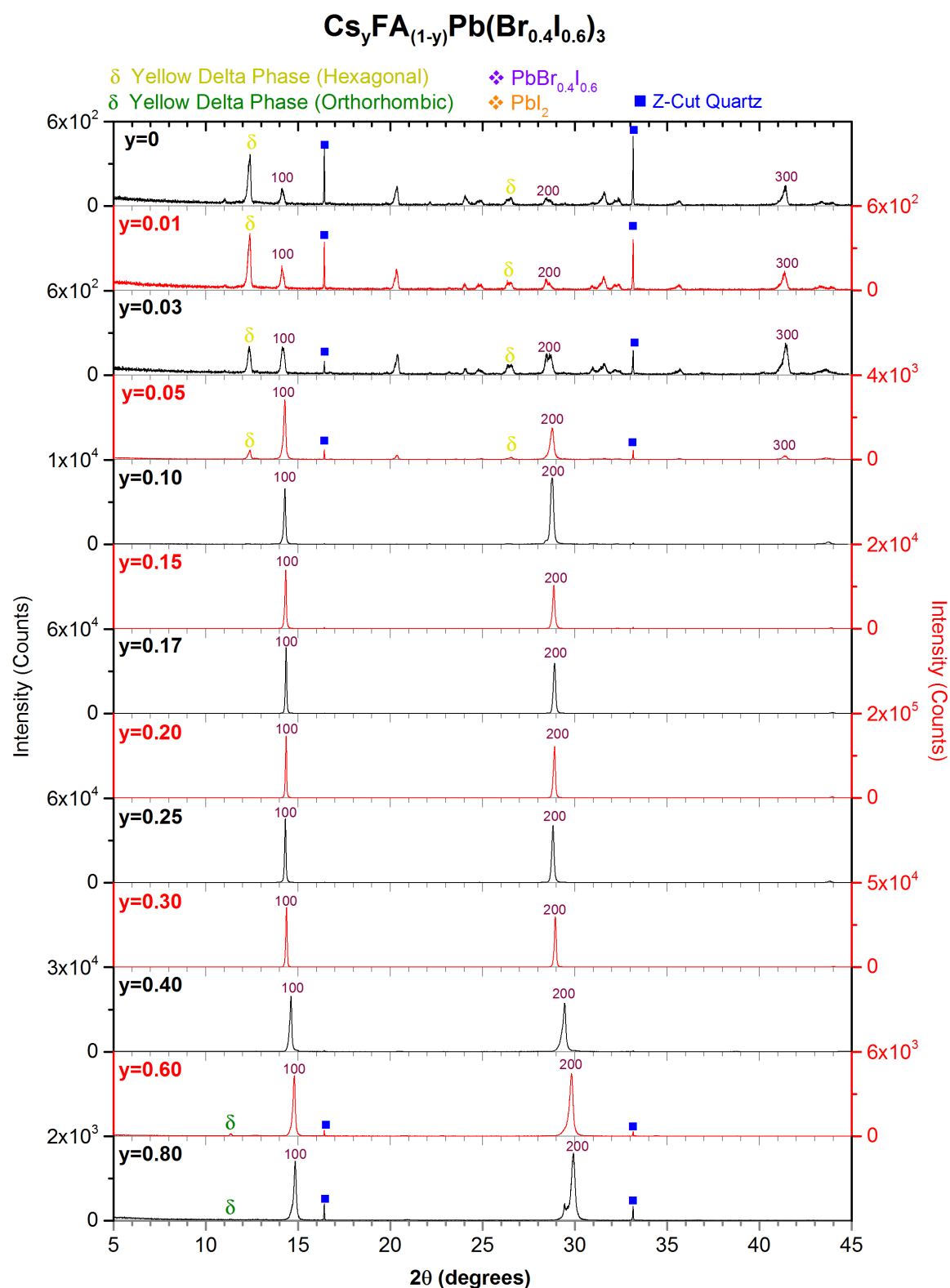


Figure S2. X-Ray Diffraction pattern of $\text{Cs}_y\text{FA}_{(1-y)}\text{Pb}(\text{Br}_{0.4}\text{I}_{0.6})_3$ thin films with varying cesium content ($0 < y < 0.8$). As the concentration of Cs reaches 30%, the Intensity of the cubic (100) reflections not only stabilizes at $2\theta \sim 14.3^\circ$ the peak intensity increases and sharpens. This is shown in more detail in figure S3

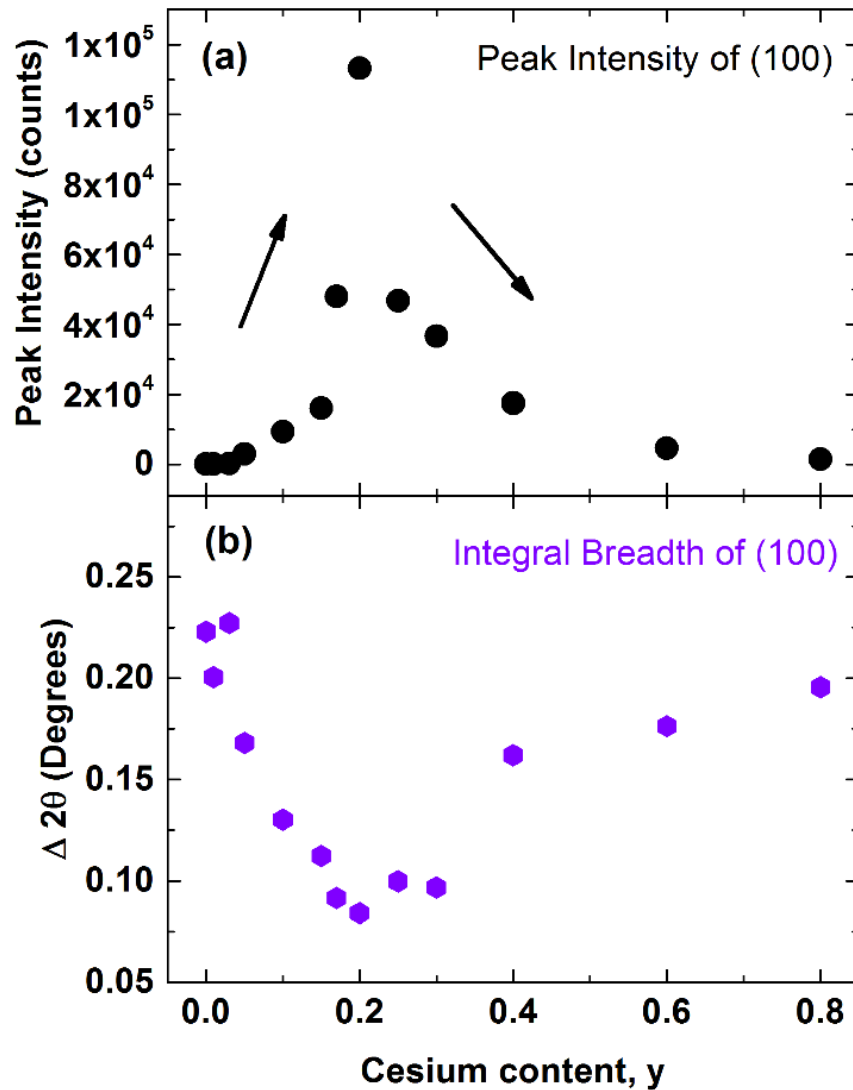


Figure S3. (a) Intensity change of the (100) reflection peak as a function of the cesium content in $\text{Cs}_y\text{FA}_{(1-y)}\text{Pb}(\text{Br}_{0.4}\text{I}_{0.6})_3$ thin films. This is clear indication of the films encompassing strong crystalline domains between Cs 17%-25%. Thereafter, further addition of Cs shows large shifts of the cubic reflection and a reduction in Intensity and broadening of the peak. **(b)** Integral Breadth of the (100) reflection peak as a function of the cesium content in $\text{Cs}_y\text{FA}_{(1-y)}\text{Pb}(\text{Br}_{0.4}\text{I}_{0.6})_3$ thin films.

C2. PL and absorption spectra for $\text{Cs}_y\text{FA}_{(1-y)}\text{Pb}(\text{Br}_{0.4}\text{I}_{0.6})_3$ films

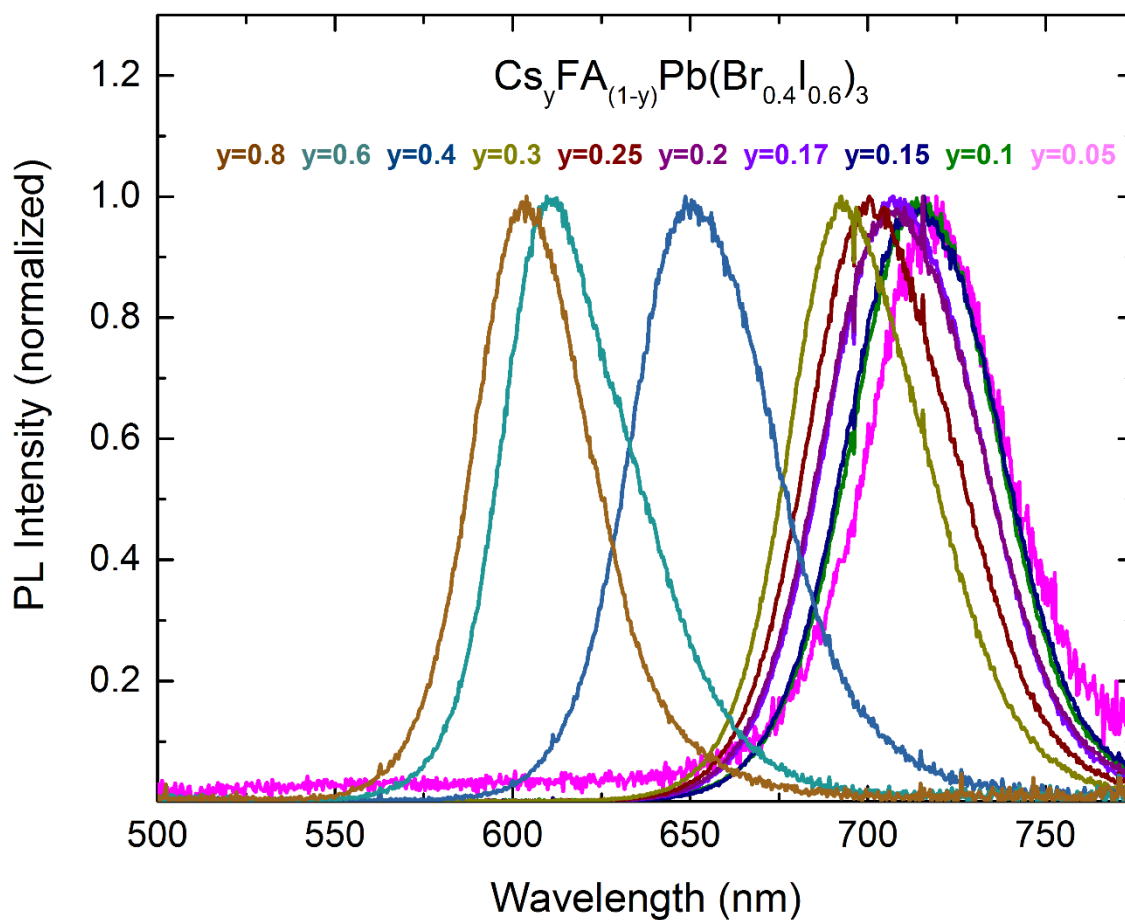


Figure S4. Steady-state photoluminescence (PL) spectra of $\text{Cs}_y\text{FA}_{(1-y)}\text{Pb}(\text{Br}_{0.4}\text{I}_{0.6})_3$ thin films with varying cesium content y , recorded immediately following excitation at 400 nm at a fluence of $13.5 \mu\text{J cm}^{-2}$ (14.9 mW cm^{-2}) under vacuum. The PL spectra have been normalized to the peak emission.

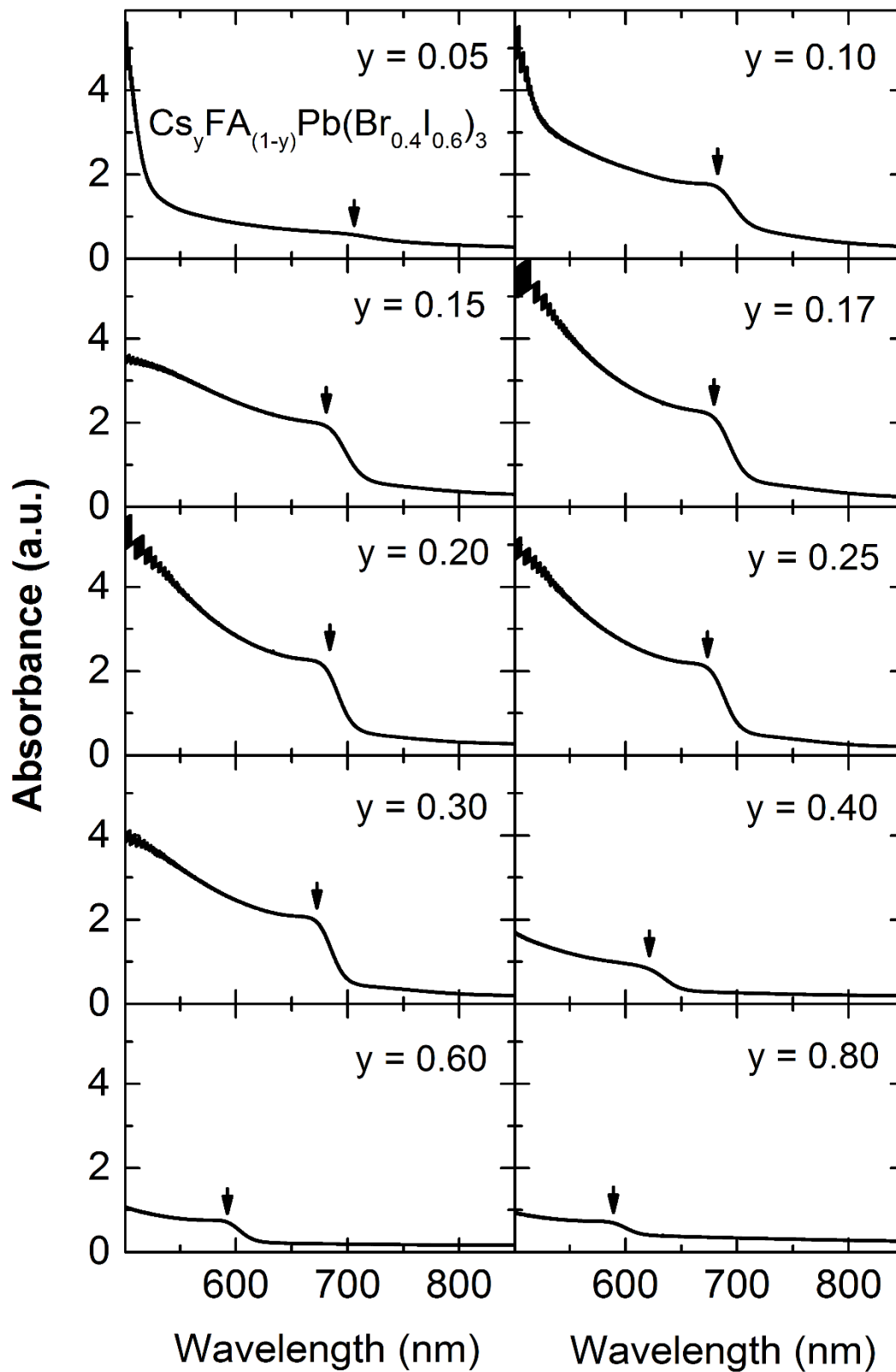


Figure S5. Absorbance spectra of $\text{Cs}_y \text{FA}_{(1-y)} \text{Pb}(\text{Br}_{0.4}\text{I}_{0.6})_3$ films with varying cesium content y . Vertical arrows indicate the absorption onsets. The data were obtained by measuring the optical transmission and reflection using a Fourier-transform infrared spectrometer.

C3. PL transients for $\text{Cs}_y\text{FA}_{(1-y)}\text{Pb}(\text{Br}_{0.4}\text{I}_{0.6})_3$ films

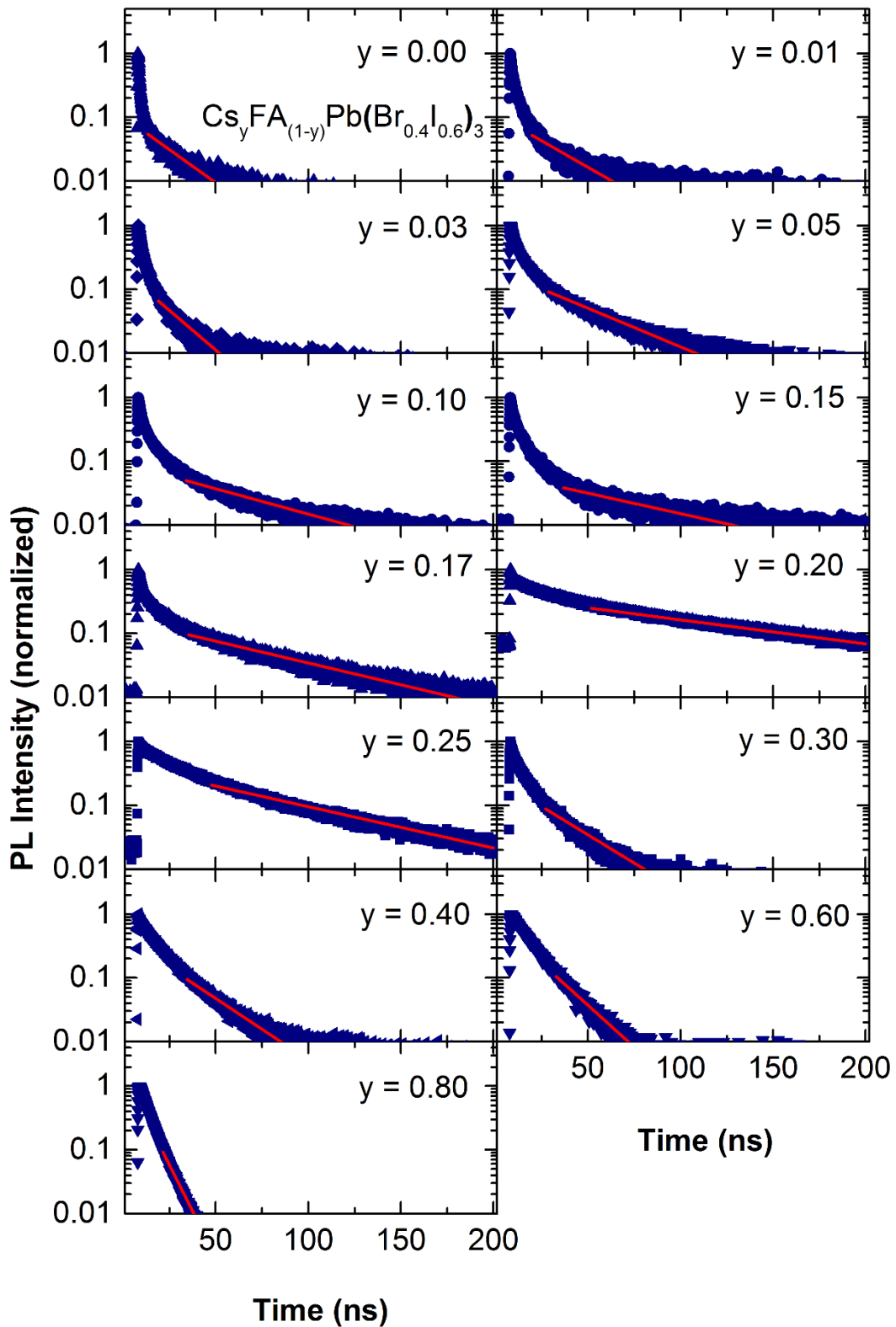


Figure S6. Time-resolved PL spectroscopy of $\text{Cs}_y\text{FA}_{(1-y)}\text{Pb}(\text{Br}_{0.4}\text{I}_{0.6})_3$ films with varying cesium content y , following excitation at 400 nm at an excitation fluence and $0.0151 \mu\text{J}/\text{cm}^2$. The laser intensity was at $2.53 \text{ W}/\text{cm}^2$. The PL decay traces have been normalized to the peak emission.

C4. PL photodegradation spectra for selected $\text{Cs}_y\text{FA}_{(1-y)}\text{Pb}(\text{Br}_{0.4}\text{I}_{0.6})_3$ films

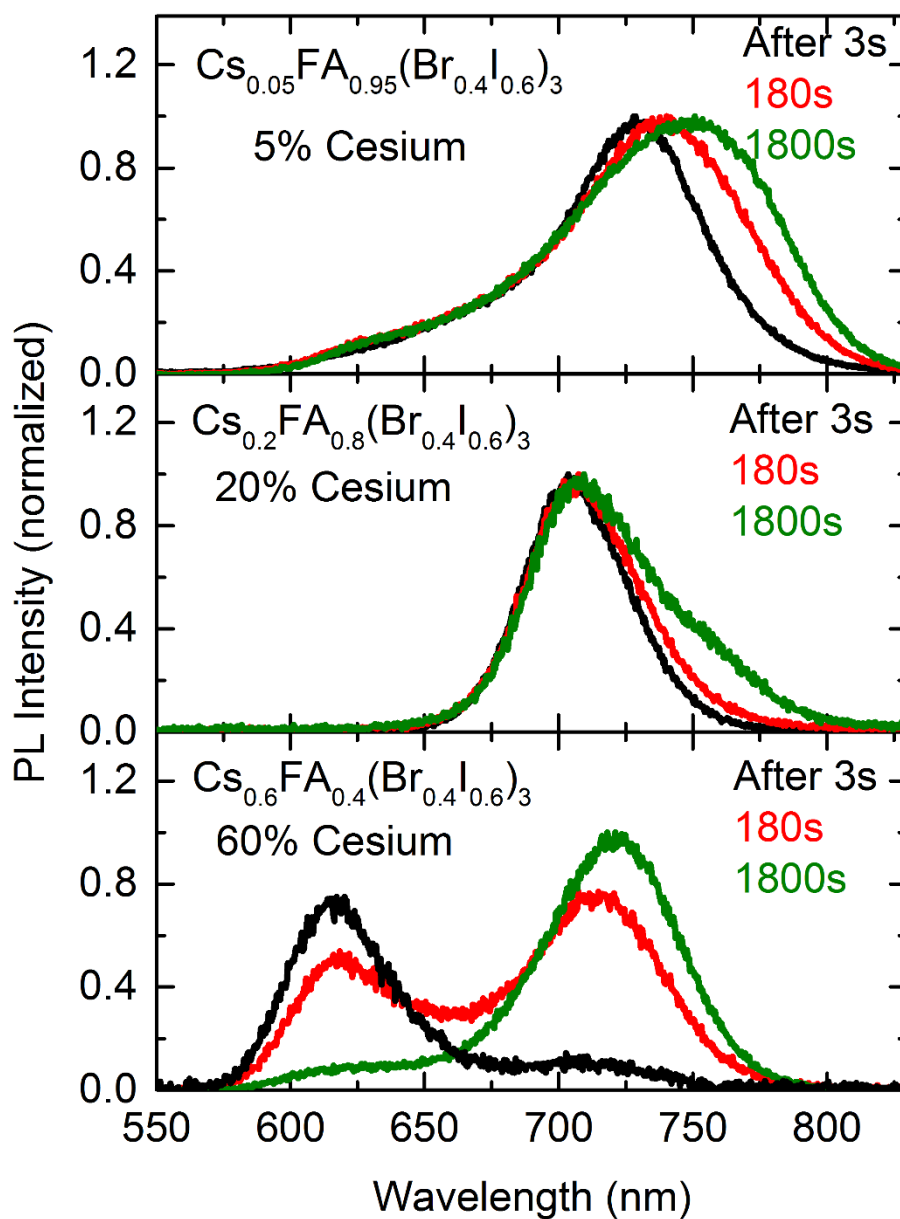


Figure S7. PL spectra of three different $\text{Cs}_y\text{FA}_{(1-y)}\text{Pb}(\text{Br}_{0.4}\text{I}_{0.6})_3$ films ($y = 0.05$, $y = 0.2$ and $y = 0.6$) over the course of 30 minutes of continuous illumination in vacuum following excitation at 400 nm at an intensity of 100 mW cm^{-2} (fluence of $0.1 \mu\text{J cm}^{-2}$, pulse duration 100 fs, repetition rate 80 MHz). The PL spectra have been normalized to the peak emission.

D. Further characterization data for $\text{Cs}_{0.17}\text{FA}_{0.83}\text{Pb}(\text{Br}_x\text{I}_{1-x})_3$ films

D1. PL transients for $\text{Cs}_{0.17}\text{FA}_{0.83}\text{Pb}(\text{Br}_x\text{I}_{1-x})_3$ films

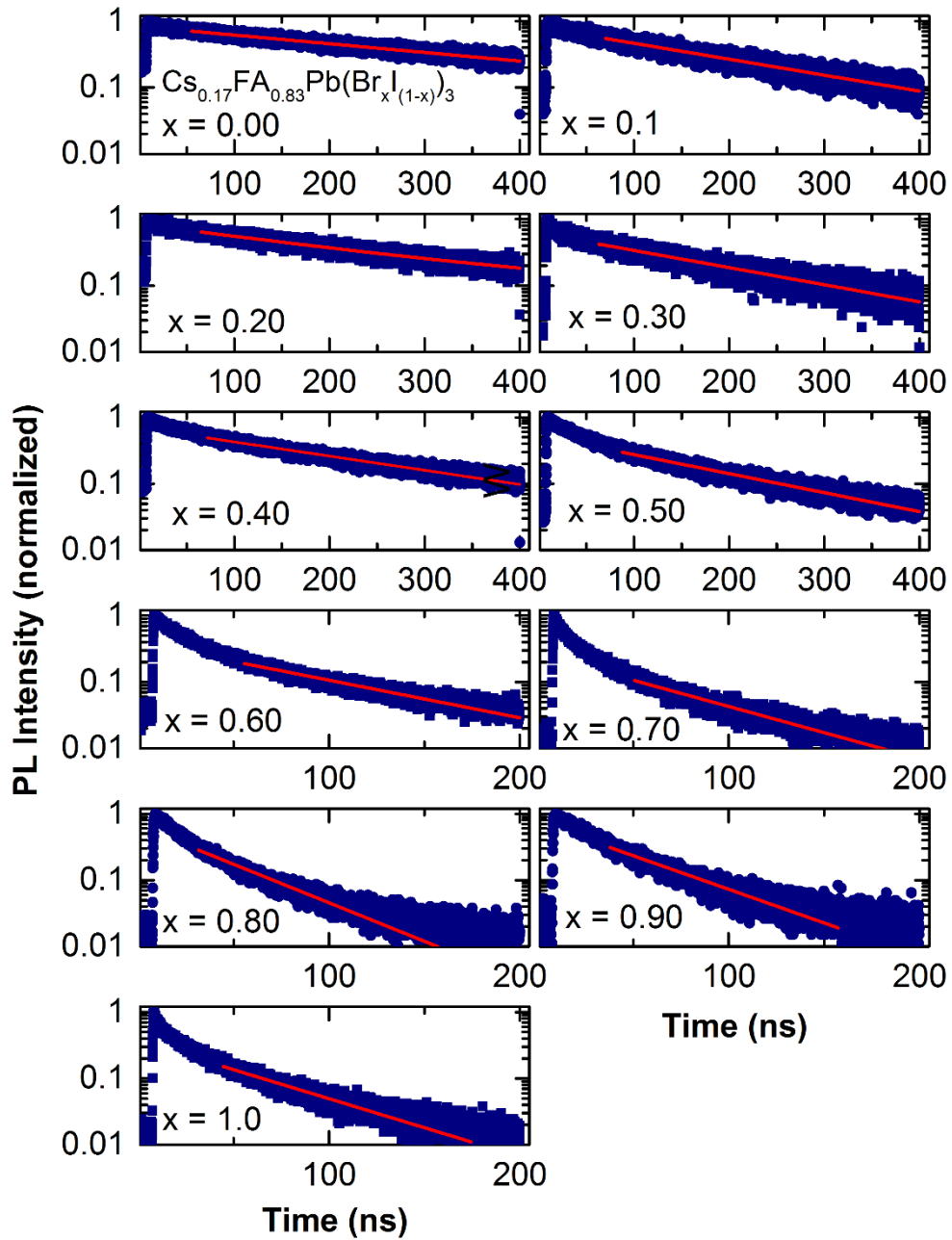


Figure S8. Time-resolved PL spectroscopy of $\text{Cs}_{0.17}\text{FA}_{0.83}\text{Pb}(\text{Br}_x\text{I}_{1-x})_3$ films with varying bromide content x , following excitation at 400 nm at a low excitation fluence of $0.015 \mu\text{J}/\text{cm}^2$. The laser intensity was at $2.53 \text{ W}/\text{cm}^2$. The PL decay traces have been normalized to the peak emission.

D2. THz photoconductivity transients for $\text{Cs}_{0.17}\text{FA}_{0.83}\text{Pb}(\text{Br}_x\text{I}_{1-x})_3$ films

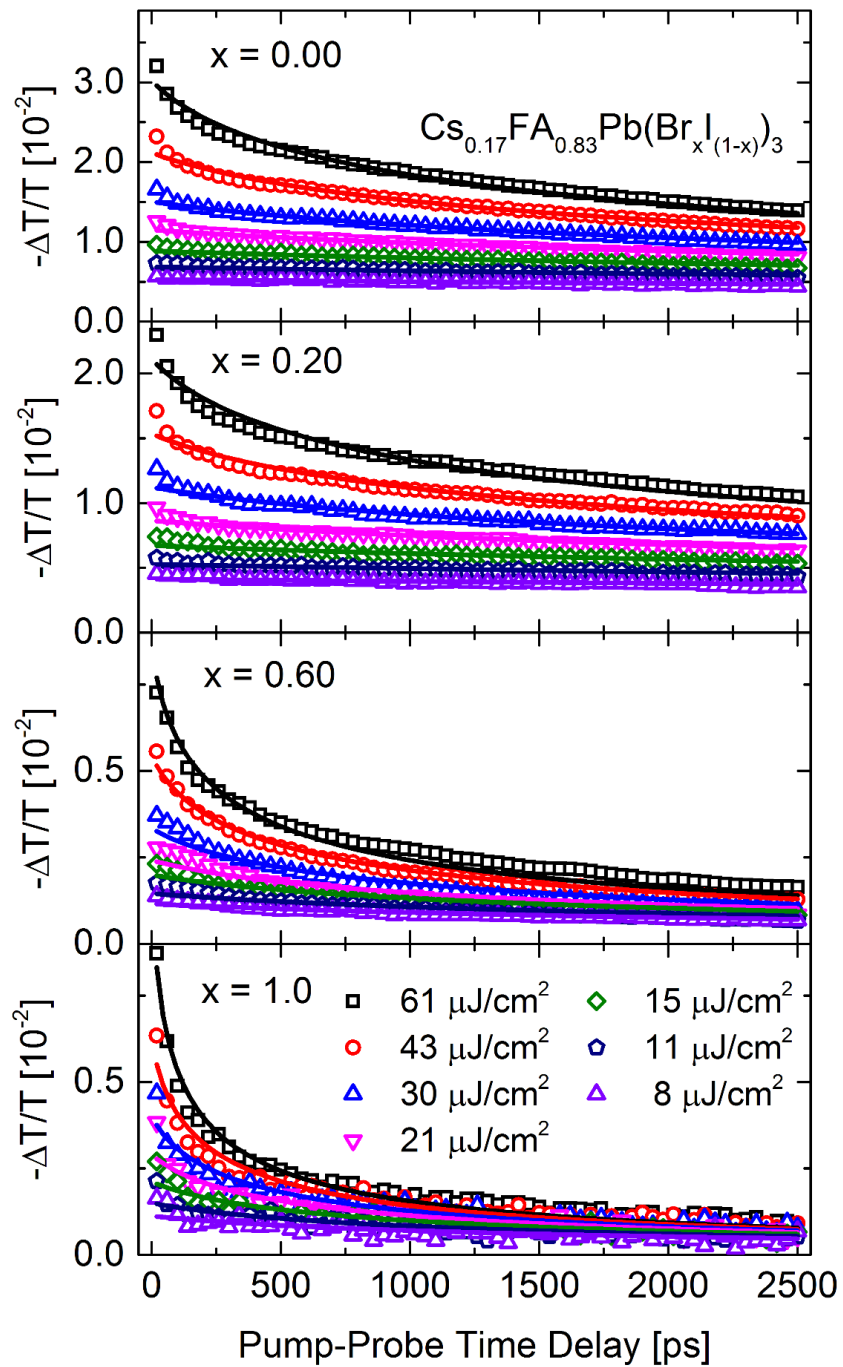


Figure S9. THz photoconductivity transients in thin films of $\text{Cs}_{0.17}\text{FA}_{0.83}\text{Pb}(\text{Br}_x\text{I}_{1-x})_3$ with a) $x = 0.0$, b) $x = 0.20$, c) $x = 0.60$ and d) $x = 1$, for excitation fluences between $8 \mu\text{J}/\text{cm}^2$ and $61 \mu\text{J}/\text{cm}^2$ at an excitation wavelength of 400nm . The symbols represent data points, and the solid lines are fits as described above in Section B2.

D3. PL and absorption spectra for $\text{Cs}_{0.17}\text{FA}_{0.83}\text{Pb}(\text{Br}_x\text{I}_{1-x})_3$ films

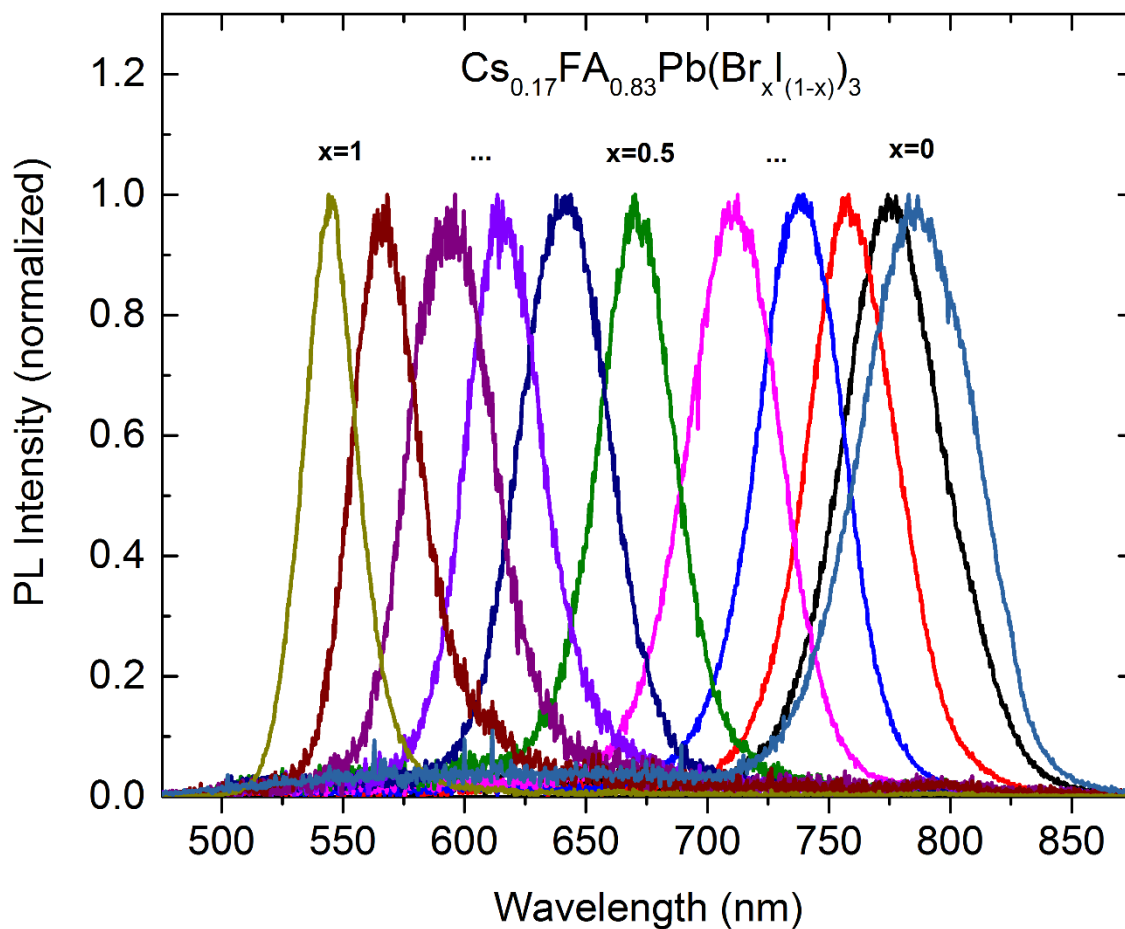


Figure S10. Steady-state photoluminescence (PL) spectra of $\text{Cs}_{0.17}\text{FA}_{0.83}\text{Pb}(\text{Br}_x\text{I}_{1-x})_3$ thin films with varying bromide content x , recorded immediately following excitation at 400 nm at a fluence of $13.5 \mu\text{J cm}^{-2}$ (14.9 mW cm^{-2}) under vacuum. The PL spectra have been normalized to the peak emission.

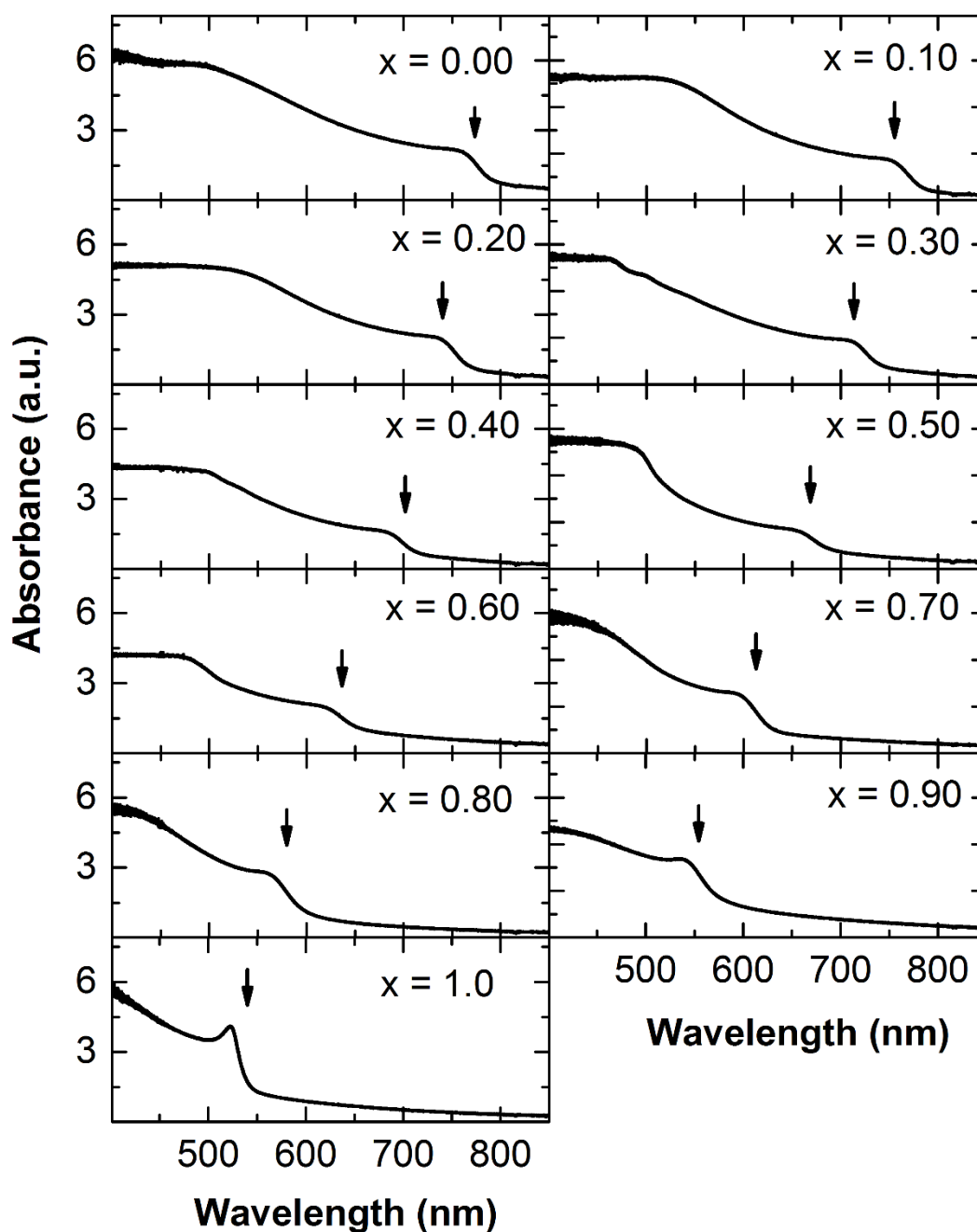


Figure S11. Absorbance spectra of $\text{Cs}_{0.17}\text{FA}_{0.83}\text{Pb}(\text{Br}_x\text{I}_{(1-x)})_3$ films with varying bromide content x . Vertical arrows indicate absorption onsets. The data were obtained by measuring the optical transmission and reflection using a Fourier-transform infrared spectrometer.

D4. Calculation of charge-carrier diffusion lengths $\text{Cs}_{0.17}\text{FA}_{0.83}\text{Pb}(\text{Br}_x\text{I}_{1-x})_3$ films

In order to further investigate the effects of mobility and recombination rate changes, the diffusion lengths L_D were calculated according to Equation (1).

$$L_D(n) = \sqrt{\frac{D}{R_{total}(n)}} \quad (10)$$

The total recombination rate R_{total} is determined by the charge-carrier density and the recombination rate constants (k_1 , k_2 , and k_3) of the individual recombination processes:

$$R_{total} = -\frac{1}{n} \frac{dn}{dt} = n^2 k_3 + nk_2 + k_1 \quad (11)$$

Here, the diffusion constant D is the product of the mobility μ , Boltzmann constant k_B , and temperature T divided by the elementary charge e :

$$D = \frac{\mu k_B T}{e} \quad (12)$$

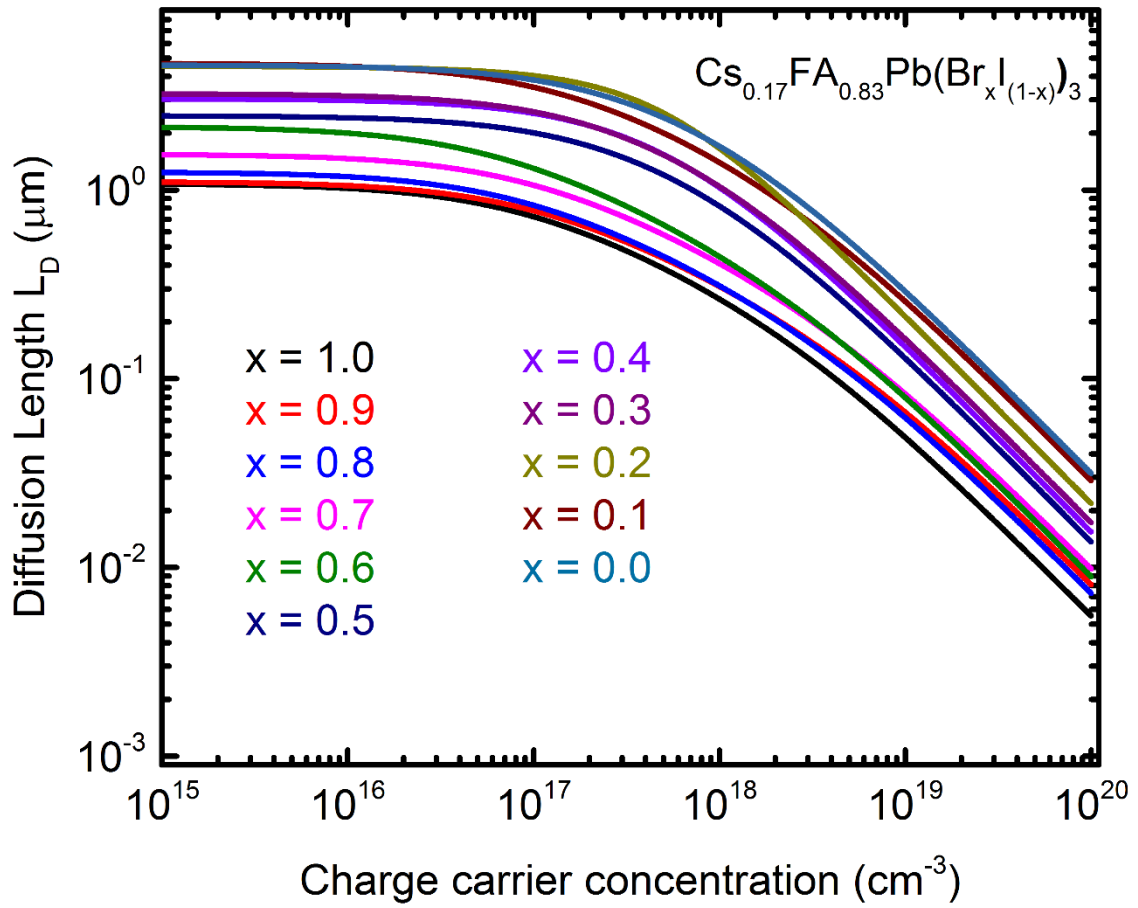


Figure S12. Charge-carrier diffusion lengths as a function of charge-carrier concentration in $\text{Cs}_{0.17}\text{FA}_{0.83}\text{Pb}(\text{Br}_x\text{I}_{(1-x)})_3$ thin films with varying bromide content x .